12th International Symposium on Turbulence and Shear Flow Phenomena (TSFP12)
Osaka, Japan (Online), July 19-22, 2022

SIMULATION OF THE TURBULENT FLOW OVER A CANOPY OF HIGHLY FLEXIBLE BLADES

Bastian Löhrer
Institute of Fluid Mechanics
Technische Universität Dresden
01062 Dresden, Germany
bastian.loehrer@tu-dresden.de

Léo Guiot de la Rochère
LMFA, CNRS – UMR 5509, Université de Lyon, École Centrale de Lyon, Université Lyon 1, INSA Lyon
Écully, France
leo.guiotdelarochere@engees.unistra.fr

Delphine Doppler
LMFA, CNRS – UMR 5509, Université de Lyon, École Centrale de Lyon, Université Lyon 1, INSA Lyon
Écully, France
delphine.doppler@univ-lyon1.fr

Sara Puijalon
Univ Lyon, Université Claude Bernard Lyon 1, CNRS, ENTPE, UMR 5023 LEHNA
69622, Villeurbanne, France
sara.puijalon@univ-lyon1.fr

Jochen Fröhlich
Institute of Fluid Mechanics
Technische Universität Dresden
01062 Dresden, Germany
jochen.froehlich@tu-dresden.de

ABSTRACT

In the present contribution, a recently developed own numerical method is used, capable of representing individual flexible vegetation elements as they reconfigure and closely interact with the surrounding flow. The method is applied to a model configuration composed of very long flexible rectangular blades whose length and high flexibility translates into a Cauchy number around 25,000. This very detailed, turbulence-resolving and plant-resolving simulation at high Cauchy number is the first of its kind, enabled by a composition of efficient numerical modeling techniques.

INTRODUCTION

Aquatic canopies formed by flexible submerged plants are an essential element in river hydraulics through the flow resistance they provide, their resilience from bed erosion, and their impact on the transport of nutrients and pollutants (Nepf, 2012). Knowledge about these processes is frequently drawn from controlled model experiments and simulations alike, employing relatively rigid elements to facilitate optical accessibility and to reduce the complexity of simulations. Long and highly flexible elements pose challenges to experiments and simulations, and are addressed here.

PHYSICAL MODEL

Subject of the presented work is the fully developed flow with bulk velocity U_b in a laterally confined open channel of width L_z. Flexible blades of length $L = L_z$ are attached perpendicular to the bottom wall at staggered locations, such that they form a dense canopy while also avoiding any channelization of the flow in between the stems. The overall problem can be characterized by the nominal Cauchy number $Ca = \rho U_\mathrm{b}^2 W L^3/(2EI)$, where $I = T^3 W/12$ is the second moment of area, the buoyancy number $B = (\rho - \rho_\mathrm{s})\, gWTL^3/(EI)$, and by Reynolds numbers $Re_H = U_\mathrm{b} H/\nu$ and $Re_W = U_\mathrm{b} W/\nu$, based on the channel height and the width of the blades, respectively.

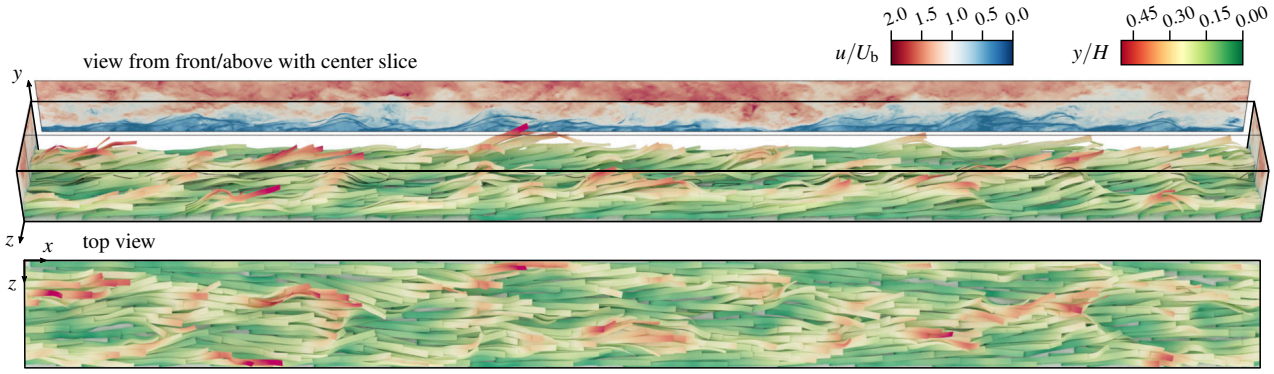

Figure 1. Visualization of an instantaneous solution, showing the streamwise velocity component u in the center plane $z = 0.5L_z$, and the instantaneous shape of the canopy with each blade colored according to the vertical position y.

The corresponding values for the present case are listed in Table 1, of which the huge value of Ca and the relatively large value of B reflect the large flexibility of the blades, i. e. nominal drag and lift forces outweighing elastic forces.

NUMERICAL METHOD

The problem was analyzed on the basis of numerical simulations using the in-house code PRIME developed at TU Dresden (Kempe & Fröhlich, 2012; Tschisgale & Fröhlich, 2020). This method solves the Navier-Stokes equations for incompressible flows employing a second-order finite volume approach on a staggered Cartesian grid for the spatial discretization and a second-order scheme for time integration. A Large Eddy Simulation (LES) approach with the Smagorinsky model was employed with damping close to the blades. In the simulation reported below, the horizontal average of the ratio of turbulent to molecular viscosity remains below 0.25. The motion of the flexible structures was computed with a finite-difference approach according to Lang & Arnold (2012), using a geometrically exact Cosserat rod model (Antman, 1995) which is suitable for large deflections. While accounting for bending, torsional, and shearing motion, the model is built upon the assumption of rigid cross sections which prevents warping. Since warping is, however, a central mechanism of deformation its effect was modeled by reducing torsional and shearing stiffnesses as proposed by Freund & Karakoç (2016). Collisions were treated based on the model proposed by Tschisgale *et al.* (2019) with several technical enhancements. Coupling between fluid and structures was established with a specialized Immersed-Boundary Method (IBM) applicable for small and even vanishing thickness of the blades, imposing a no-slip condition on the surfaces of the rods (Tschisgale & Fröhlich, 2020).

Table 1. Dimensionless numbers.

number	value	description
Ca	25,000	Nominal Cauchy number
B	145	Buoyancy number
Re_W	1922	Reynolds number
Re_H	20,064	Reynolds number
λ	0.41	Roughness density

COMPUTATIONAL MODEL

The simulation was configured according to an experiment presently conducted at the university of Lyon. The computational domain spans a length of $18.5H \approx 11.5L_z$ in streamwise direction, where H is the water depth and L_z is the spanwise extent. Periodic boundary conditions were applied in x-direction, a free-slip condition was imposed at $y = H$, and no-slip conditions were enforced at the bottom ($y = 0$) and the side walls. With a spatial resolution of 24 fluid grid cells per blade width, $\Delta x \approx W/24$, this translates into a numerical domain containing 460.8 million cells. The flow was driven by a spatially constant volume force which was adjusted in time to maintain the desired flow rate. Additional numerical parameters are provided in Table 2.

Table 2. Numerical parameters.

parameter	value	description
L_x/L	11.5	channel length per blade length
N_x	4608	cells in streamwise direction
N_y	250	cells in vertical direction
N_z	400	cells in spanwise direction
C_S	0.15	Smagorinsky constant
N_s	528	number of blades
N_e	108	number of elements per blade

RESULTS

The snapshot shown in Figure 1 above gives a first impression of the flow. Due to their remarkable flexibility and their buoyancy, the blades are oriented almost horizontally along most of their length, forming a visually dense canopy hull. This is underpinned by the roughness density λ, defined as the ratio of the mean frontal area of a plant divided by its share of the the bed area (Wooding *et al.*, 1973), listed in Table 1. A value of λ well above 0.1 indicates a dense canopy (Nepf, 2012). The observed reconfigured canopy height $L^* \approx 0.24H$ places the case in the regime of shallow submergence, $H > L^* > H/5$ where canopy scale turbulence dominates and boundary layer turbulence is usually not de-

veloped (Nepf, 2012). The canopy hull is occasionally broken open by high-speed streaks, extending all the way to the channel bed and making the blades form ridges to either side. The blades, hence, undergo a pronounced meandering motion in spanwise direction, while also undulating vertically. Their mean height, computed as the maximum elevation of their time-averaged shape (i.e. the height of their tips), is indicated in Figures 4*a-b*,*e-g* (broken line). Away from the side walls, the resulting profile coincides with an iso-contour of the streamwise mean-velocity component $\langle u \rangle$, and with the line of maximum $\langle u'u' \rangle$ in Figure 4*e*. The averaged streamwise velocity is maximum in the upper quarter of the channel between the two counter-rotating swirls in the secondary flow below the free surface, recognizable in Figure 4*b*. The symmetry-plane profile of mean streamwise velocity in figure 4*c* has a narrow region with $\langle u \rangle \approx$ const. within the canopy and two inflections points related to the drag of the blades. In contrast to situations with stiffer blades (Nepf, 2012), the second inflection point is not located at the height of the canopy edge, but instead occurs considerably lower.

The dynamic behavior of the blades is analyzed by studying the motion of their centerlines. The points along the skeleton line of a blade are $\boldsymbol{c}_s(l,t)$, depending on time, and the arc length distance l from the respective fixed end of the blade, $\boldsymbol{c}_{s0} = \boldsymbol{c}_s(0,t) = \text{const.}$ Here, s is the index of the respective blade. Defining the geometries relative to their roots, $(x_s, y_s, z_s)^{\mathrm{T}} = \boldsymbol{c}_s(l,t) - \boldsymbol{c}_{s0}$, Figure 2*a* shows the average shapes of the blade centerlines, while the root-mean-square deviations from this mean geometry are visualized in Figures 2*b-d*. Here, the pronounced spanwise fluctuations are striking. They reflect the secondary flow structures in Figure 4*b*. In a first attempt to identify frequencies associated with blade motion, spectra were computed for the spanwise and vertical coordinates of the tips of blades (Figure 3). They exhibit a broad range of frequencies without any remarkable peak, other than for a frequency linked to the flow-through time.

Autocorrelations of streamwise velocity fluctuations

$$\rho_{u'u'}(y,z;\boldsymbol{r}) = \frac{\langle u'(\boldsymbol{x},t)\, u'(\boldsymbol{x}+\boldsymbol{r},t)\rangle_{x,t}}{\sqrt{\langle u'^2(\boldsymbol{x},t)\rangle_{x,t}\ \langle u'^2(\boldsymbol{x}+\boldsymbol{r},t)\rangle_{x,t}}}$$

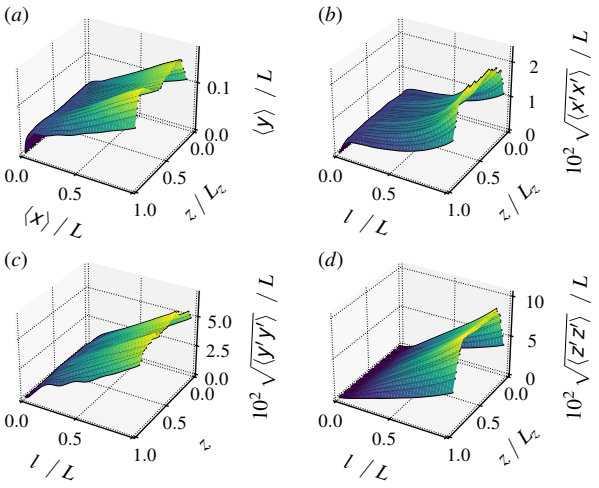

Figure 2. One-point statistics of the geometry of the blade skeleton lines depending on the z-location of their fixed roots. (*a*) Mean geometry of the blades; (*b-d*) root-mean-square values of their deviation from the mean shapes, showing x, y and z-components separately.

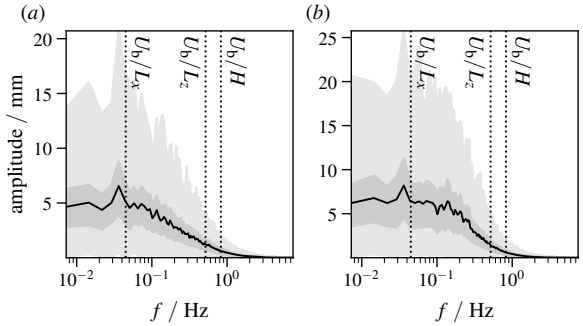

Figure 3. Amplitude spectra for the position of blade tips, i.e. at $l = L$. (*a*) Spanwise component; (*b*) vertical component. Spectra were computed per blade, then averaged across the blades to obtain the solid black line. The gray areas span the range of all and of 50 % of the spectra, respectively. Frequencies associated with the channel dimensions are indicated by the dotted lines.

are shown in Figure 5*a*, manifesting an inclined, elliptical pattern, elongated in streamwise direction. Vertical velocity fluctuations are only correlated over a significantly shorter distance (Figure 5*b*) resulting in the well-known spherical pattern also observed by Shaw *et al.* (1995).

CONCLUSIONS

Scale-resolving simulations of the flow over highly flexible, resolved vegetation elements, give access to a broad range of data, including field quantities related to the flow, and related to the motion of the blades. Despite being characterized by a pronounced secondary flow due to the fixed side walls, statistics are relatively constant in a core region of the channel geometry. Yet, future investigations are to feature wider domains with spanwise periodicity. Although the blades form a dense canopy surface which undulates under the flow, none of these apparent frequencies are present in spectra of blade tip motion. This indicates, that pointwise blade motion statistics provide only a limited window into the motion of the canopy. It may thus be more insightful to inspect the continuous canopy hull formed by the union of all blades.

ACKNOWLEDGEMENTS

This work was funded by the French-German ANR-DFG project ESCaFlex (ANR-16-CE92-0020, DFG grant 634058). Computation time was provided by ZIH Dresden.

REFERENCES

Antman, S. S. 1995 *Nonlinear Problems of Elasticity*, *Applied Mathematical Sciences*, vol. 107. New York, NY: Springer New York.

Freund, J. & Karakoç, A. 2016 Warping displacement of Timoshenko beam model. *International Journal of Solids and Structures* **92–93**, 9–16.

Kempe, T. & Fröhlich, J. 2012 An improved immersed boundary method with direct forcing for the simulation of particle laden flows. *Journal of Computational Physics* **231** (9), 3663–3684.

Lang, H. & Arnold, M. 2012 Numerical aspects in the dynamic simulation of geometrically exact rods. *Applied Numerical Mathematics* **62** (10), 1411–1427.

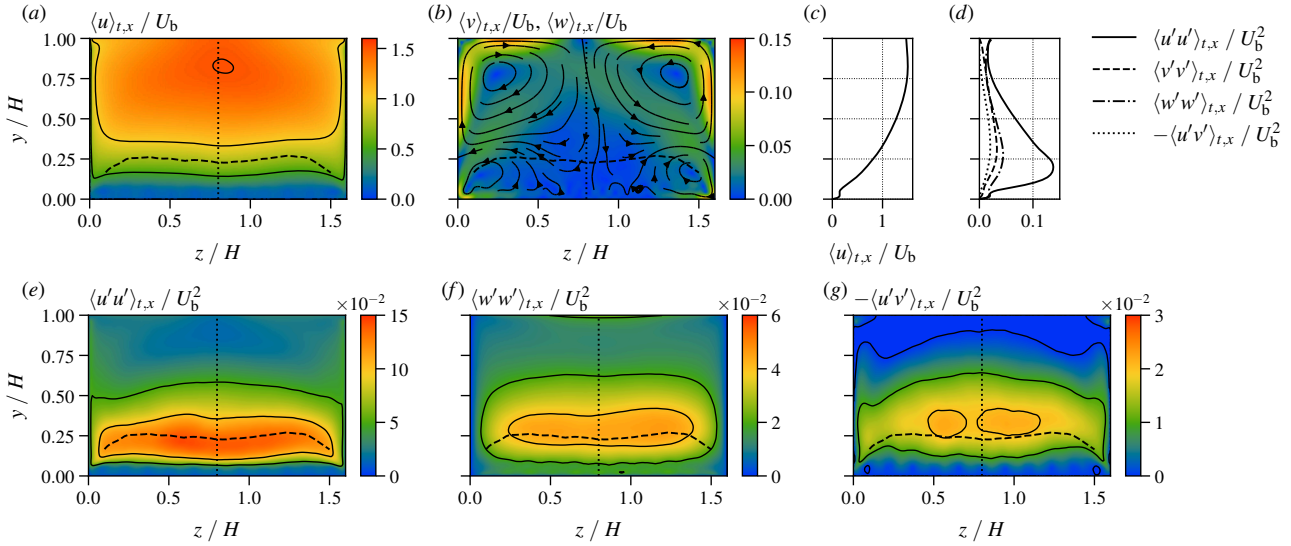

Figure 4. One-point statistics of the fluid motion in the channel cross section and profiles located at the vertical center line $z = 0.5L_z$. (*a*) mean streamwise velocity; (*b*) mean secondary flow with streamlines and magnitude of secondary velocity components; (*c*) mean streamwise velocity in center plane; (*d*) Reynolds stresses in center plane; (*e-g*) Reynolds stresses, as indicated. In the contour plots, the broken lines represent the average canopy height corresponding to the vertical position of the time-averaged blade geometries. $\langle\cdot\rangle_{t,x}$ denotes averaging in time, followed by averaging in the periodic x-direction, while $u' = u - \langle u\rangle_t$ is the deviation from the local time average $\langle\cdot\rangle_t$.

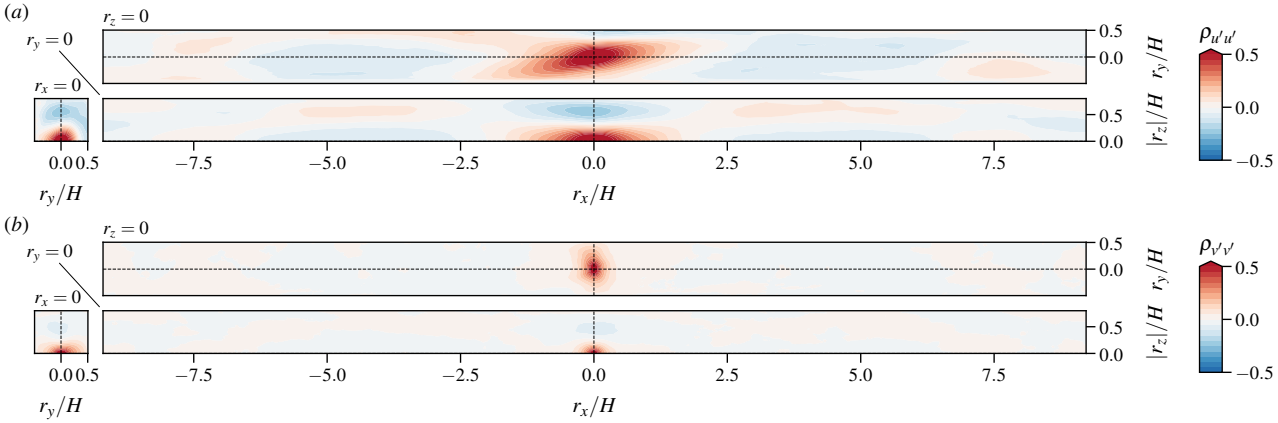

Figure 5. Two-point correlations of velocity fluctuations, computed for the center of the channel cross section, i.e. $y = 0.5H$, $z = 0.5L_z$. (*a*) streamwise velocity component; (*b*) vertical velocity component.

Nepf, H. M. 2012 Flow and Transport in Regions with Aquatic Vegetation. *Annual Review of Fluid Mechanics* **44**, 123–142.

Shaw, R. H., Brunet, Y., Finnigan, J. J. & Raupach, M. R. 1995 A wind tunnel study of air flow in waving wheat: Two-point velocity statistics. *Boundary-Layer Meteorology* **76** (4), 349–376.

Tschisgale, S. & Fröhlich, J. 2020 An immersed boundary method for the fluid-structure interaction of slender flexible structures in viscous fluid. *Journal of Computational Physics* **423**, 109801.

Tschisgale, S., Thiry, L. & Fröhlich, J. 2019 A constraint-based collision model for Cosserat rods. *Archive of Applied Mechanics* **89** (2), 167–193.

Wooding, R. A., Bradley, E. F. & Marshall, J. K. 1973 Drag due to regular arrays of roughness elements of varying geometry. *Boundary-Layer Meteorology* **5** (3), 285–308.